

# Effective 90-degree magnetization rotation in Co<sub>2</sub>FeAl thin film/piezoelectric system probed by microstripline ferromagnetic resonance

M. Gueye,<sup>1</sup> F. Zighem,<sup>1</sup> M. Belmeguenai,<sup>1</sup> M. S. Gabor,<sup>2</sup> C. Tiusan,<sup>2</sup> and D. Faurie<sup>1</sup>

<sup>1</sup>LSPM-CNRS, Université Paris XIII, Sorbonne Paris Cité, 93430 Villetaneuse, France

<sup>2</sup>Center for Superconductivity, Spintronics and Surface Science, Technical University of Cluj-Napoca, Str. Memorandumului No. 28, RO-400114 Cluj-Napoca, Romania

(Received 23 May 2015; accepted 12 July 2015; published online 22 July 2015)

Microstripline ferromagnetic resonance technique has been used to study the indirect magnetoelectric coupling occurring in an artificial magnetoelectric heterostructure consisting of a magnetostrictive thin film cemented onto a piezoelectric actuator. Two different modes (sweep-field and sweep-frequency modes) of this technique have been employed to quantitatively probe the indirect magnetoelectric coupling and to observe a voltage induced magnetization rotation (of 90°). This latter has been validated by the experimental frequency variation of the uniform mode and by the amplitude of the sweep-frequency spectra. © 2015 AIP Publishing LLC. [<http://dx.doi.org/10.1063/1.4927308>]

In recent decades, the development and the sophistication of growth and characterization on the atomic and nanometric scale have led to the elaboration of smart materials which reveal captivating phenomena. In the midst of these materials, multiferroics magnetoelectric materials, currently at the cutting edge of spintronics, have attracted the attention of many groups.<sup>1–5</sup> A flurry of research activities has been launched in order to explore the physics behind these materials. From the applications standpoint, an alternative approach to overcome the scientific impediments of weak magnetoelectric coupling in single-phase multiferroics is two-phase systems of ferromagnetic and ferroelectric constituents.<sup>6</sup> One of the major advantages of ferromagnetic/ferroelectric extrinsic multiferroics, as reported in the literature, is the flexibility in the choice of the materials.<sup>6</sup> One of the main ideas behind the fabrication of artificial magnetoelectric multiferroics is the electric or voltage control of the magnetization using electric fields for low power and ultra fast next generation electronics.<sup>7,8</sup> The straightforward heterostructure allowing such a control appears to be the one presenting a piezoelectric/magnetostrictive interface wherein the interaction vector is the voltage induced in-plane strains.<sup>6,9–14</sup>

The present study concerns the experimental observation of the voltage induced magnetization rotation in an artificial magnetoelectric heterostructure by probing the magnetic resonance of the uniform precession mode. A method based only on microstripline ferromagnetic resonance (MS-FMR) experiments is presented.<sup>15</sup> The two different modes of this technique are presented and used to perform a quantitative characterization of the effective magnetoelectric coupling, as well as of the voltage induced magnetization-rotation. Figures 1(a) and 1(b) show the artificial heterostructure composed of a 25 nm Co<sub>2</sub>FeAl (CFA) thin film grown onto a 125 μm thick polyimide (Kapton®) flexible substrate and then cemented on a piezoelectric actuator. The CFA film was deposited onto the Kapton® substrate by rf sputtering. The deposition residual pressure was of around  $4 \times 10^{-9}$  mbar, while the working Ar pressure was of  $1.3 \times 10^{-3}$  mbar. A 5 nm thick Ta cap layer was deposited on the top of the CFA film in order to protect it from oxidation.

CFA was chosen because of its non-negligible magnetostriction coefficient at saturation even in a polycrystalline film with no preferred orientation ( $\lambda \approx 14 \times 10^{-6}$ ),<sup>16,17</sup> which will produce strong indirect magnetoelectric field and also because it is a serious candidate for spintronic applications.<sup>18–20</sup> Moreover, we have shown that Kapton substrate does not affect the whole system magnetoelectric behavior because of its high compliance.<sup>9,11</sup>

MS-FMR experiments can be carried out in two different modes: (i) by fixing the microwave driving frequency ( $f_0$ ) and sweeping the applied magnetic field ( $H$ )<sup>11,15,18</sup> or (ii) by fixing the applied magnetic field ( $H_0$ ) and sweeping the microwave frequency ( $f$ ).<sup>21</sup> A resonance field ( $H_{res}$  at fixed  $f_0$ ) and a resonance frequency ( $f_{res}$  at fixed  $H_0$ ) are extracted from these two modes each having their own advantage. Indeed, the sweep-field mode is more sensitive than the sweep-frequency one (both modes are of course less sensitive than standard FMR technique where resonant microwave cavities are used). However, contrary to the sweep-field mode, the sweep-frequency mode presents the advantage of performing spectra without disturbing the magnetization distribution of the studied systems,<sup>22</sup> provided that the rf field  $\vec{h}_{rf}$  amplitude is weak enough (which is the case here). These two modes have been used in the present study to characterize the indirect magnetoelectric field and to probe the voltage induced magnetization rotation.

A beforehand characterization of the magnetic properties of the heterostructure has been performed in the benchmark state (i.e., absence of applied voltage) in order to measure the effective magnetization ( $M_{eff}$ ) and the gyromagnetic factor ( $\gamma$ ) as well as the unavoidable uniaxial anisotropy ( $H_u$ ) due to in-plane non-equibiaxial residual stresses. This initial anisotropy is attributed to imperfect flatness of the Kapton substrate during deposition and/or cementation on the actuator.<sup>9</sup> The quantitative evaluation of this initial uniaxial anisotropy is performed through the angular dependence of the uniform mode resonance field (see Figure 1(c)) measured at  $f_0 = 10$  GHz.<sup>15</sup> Furthermore, one can note that this anisotropy is aligned along the y-axis since the resonance field minimum reaches a minimum at  $\varphi_H = 90^\circ$ . In

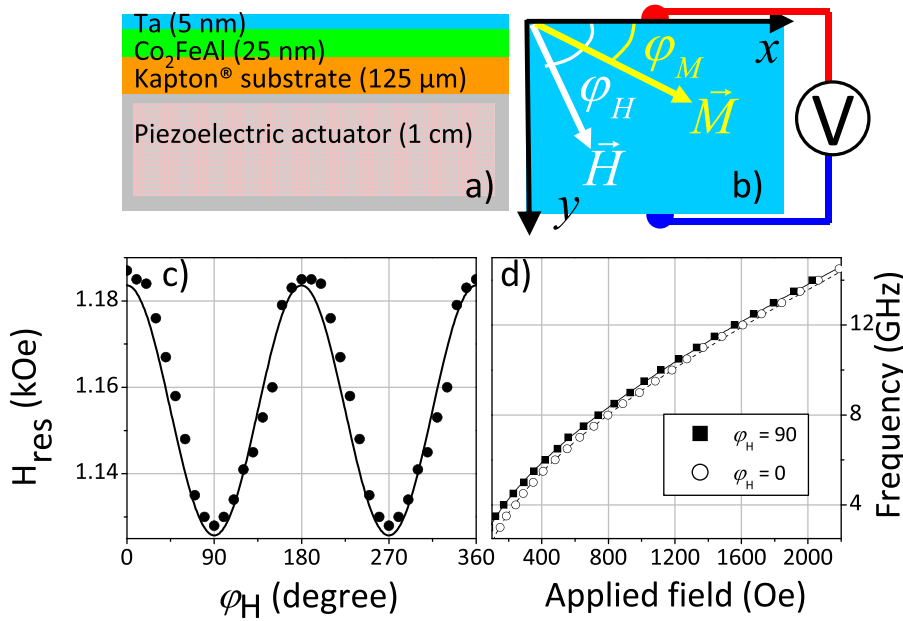


FIG. 1. (a) Depiction of the cross section view of the investigated system illustrating the CFA/Kapton<sup>®</sup> system deposited onto a piezoelectric actuator. (b) Top view sketch of the system showing the different angles used in the text. (c) Angular dependence of the resonance field measured at 10 GHz. (d) Experimental and calculated frequency dependence of the uniform mode measured along the easy and hard axes ( $\varphi_H = 90^\circ$  and  $\varphi_H = 0^\circ$ ).

addition, the frequency dependencies of the uniform mode, measured along the easy ( $\varphi_H = 90^\circ$ ) and hard ( $\varphi_H = 0^\circ$ ) axes are shown in Figure 1(d). The full lines in Figures 1(c) and 1(d) are the best fits to the experimental data and allowed the determination of the following parameters:  $M_{eff} = 720 \text{ emu cm}^{-3}$ ,  $\gamma = 1.835 \times 10^7 \text{ Hz Oe}^{-1}$ , and  $H_u \sim 30 \text{ Oe}$ , which are close to the values previously obtained for similar films.<sup>16</sup>

Sweep-field MS-FMR spectra have been recorded as a function of the applied voltage (for  $f_0 = 10 \text{ GHz}$ ). This latter was varied from 0 V to 200 V by 10 V steps. Figure 2 presents typical spectra measured at different applied voltages (0 V, 100 V, and 200 V) with an applied magnetic field along y axis ( $\varphi_H = 90^\circ$ , i.e., along the initial easy axis). A shift of the resonance field, defined as  $\delta H_{res} = H_{res}(V) - H_{res}(0)$ , is clearly observed. The voltage dependence of  $\delta H_{res}$  is shown in Figure 2, where the solid line corresponds to a linear fit showing that  $\delta H_{res}$  is positive and almost proportional to V.

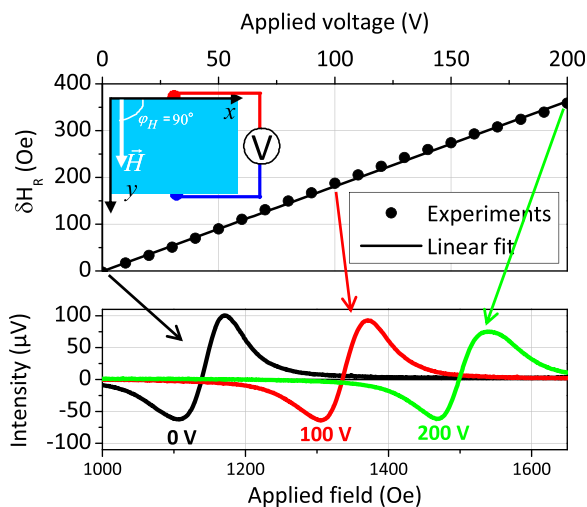


FIG. 2. Up-graph: Resonance field shift ( $\delta H_{res} = H_{res}(V) - H_{res}(0)$ ) variation as function of the applied voltage. Circles refer to experimental data, while solid line represents to the best fit. Down-graph: typical MS-FMR spectra recorded at different applied voltages (0 V, 100 V, and 200 V).

This means that the y direction gradually becomes a hard magnetization axis or a less easy one for the magnetization direction.<sup>11,15,17</sup> This is due to the positive magnetostriction coefficient of  $\text{Co}_2\text{FeAl}$  (Refs. 16 and 17) and to the nearly uniaxial tensile stress (i.e.,  $\sigma_{xx}(V) > 0$ ) along the x direction applied by the piezoelectric actuator to the film (for this range of applied voltage: 0–200 V (Ref. 23)). Note that a non-linear and hysteretic behavior is observed if the voltage is applied backward from 200 V to 0 V (not shown here) due to the intrinsic properties of the piezoelectric material.<sup>9–11,15,23</sup> It should be noted that the  $\delta H_{res}(V)$  curve presented in Figure 2 has been measured several times and all the obtained curves were superimposed. Furthermore, the resonance field shift can also be viewed as an indirect magnetoelectric field  $H_{me}(V) = \delta H_{res}(V)$  aligned along x direction, i.e., perpendicular to the initial easy axis induced by the deposition conditions. The evaluation of the voltage dependence of  $H_{me}$  will serve to quantitatively study the magnetization rotation using the sweep-frequency mode of the MS-FMR setup.

The sweep-frequency-mode has been used to probe the magnetization direction as function of the applied voltage by measuring both the resonance frequency and the spectra amplitudes. For this purpose, the selective rule, as illustrated in Figure 3, has been used. In this figure, two spectra performed with a similar applied magnetic field (of 500 Oe) along y are presented; the only difference comes from the direction of the weak rf field  $\vec{h}_{rf}$  (also called pumping field) emanating from the microstripline, which is either parallel ( $\vec{h}_{rf} \parallel \vec{M}$ ) or perpendicular ( $\vec{h}_{rf} \perp \vec{M}$ ) to the static magnetization. Indeed, the efficiency of the pumping field is maximum when  $\vec{h}_{rf} \perp \vec{M}$  (Figure 3(b)) and minimum when  $\vec{h}_{rf} \parallel \vec{M}$  (Figure 3(b)). In the present experimental conditions, a factor of 20 is found between these two geometries. Furthermore, Council *et al.*<sup>24,25</sup> demonstrated both theoretically and experimentally that for a pure Lorentzian profile of the signal, the amplitude of this signal is directly proportional to  $\sin^2 \varphi$ , where  $\varphi$  is the angle between the pumping field and the static magnetization direction. Therefore, the voltage-induced

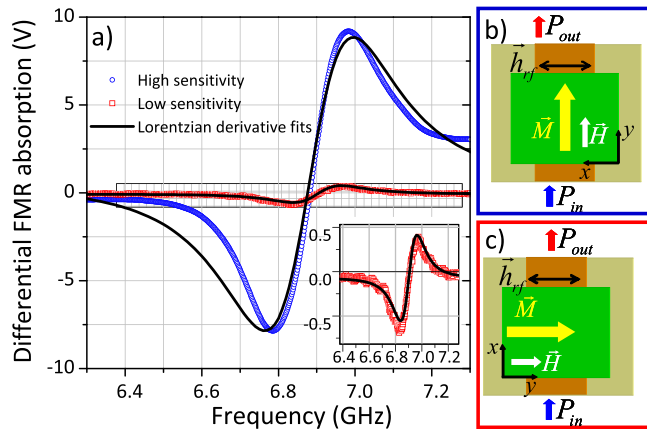


FIG. 3. (a) Sweep-frequency FMR spectra obtained according to the two configurations depicted in (b) and (c), where  $P_{in}$  and  $P_{out}$  are the injected and transmitted radio frequency current, respectively. The only difference comes from the pumping field ( $\vec{h}_{rf}$ ) which either parallel (red squares) or perpendicular (blue circles) to  $\vec{M}$  direction giving rise to the high and low sensitivities geometries. The inset shows a zoom of the marked area. Note that a saturating field of 500 Oe was applied to ensure a uniform magnetization distribution. The solid lines show fits to the first derivative of the standard Lorentzian curve.

rotation of the magnetization has been probed by measuring the evolution of the relative amplitude of the signal as function of the applied voltage.

For this purpose, the pumping field was applied parallel to  $x$  direction ( $\vec{h}_{rf} \parallel \vec{x}$ ), i.e., perpendicular to the initial easy axis (see Figure 1). In order to ensure an initial uniform magnetization along the  $y$  axis (initial easy axis), a small bias field of 40 Oe was applied. In this condition and in absence of applied voltage,  $\vec{M}$  is supposed to be uniform and aligned along  $y$  axis. Then, the voltage applied to the actuator, in steps of 10 V, leads to the development of an indirect magnetoelectric field parallel to the  $x$  axis, which tends to align  $\vec{M}$  along this axis. The normalized component of the magnetization along the indirect magnetoelectric field  $m_x(H_{me})$  is represented in Figure 4 using the following formula deduced from the model presented by Council *et al.*:<sup>24</sup>

$$m_x(H_{me}) = \frac{\cos\left(\arcsin\left(\sqrt{A_N(V)}\right)\right)}{\cos\left(\arcsin\left(\sqrt{A_N(150V)}\right)\right)}, \quad (1)$$

where  $A_N(150V)$  and  $A_N(V)$  are the normalized (by the 0 V amplitude spectrum) amplitude of the 150 V spectrum and of the applied voltage spectra, respectively. The red solid line in Figure 4 corresponds to the theoretical value of the normalized  $x$ -component of the magnetization as function of  $V$ . One can note that the rotation is complete at around 40 V ( $H_{me} = 70$  Oe), where the magnetoelectric field totally compensates the small bias field ( $H_b = 40$  Oe) and the initial anisotropy field (30 Oe). The confrontation between the model and the experimental data proves that a voltage induced magnetization rotation has been performed. Another proof of the effective rotation of the magnetization comes from the voltage dependence of the uniform mode frequency as function of the applied voltage. The blue solid line in Figure 4 refers to the simulation of this frequency being given the

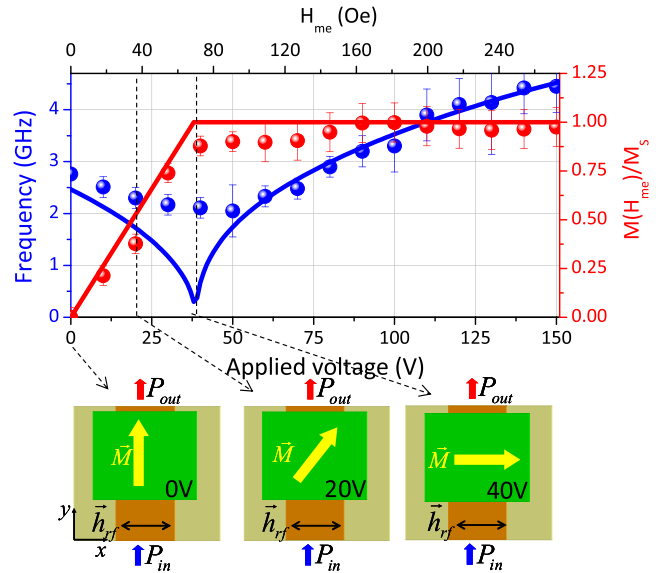


FIG. 4. Voltage dependencies of the uniform mode frequency (blue symbols) and of the normalized  $x$ -component of the magnetization  $m_x(H_{me})$  along  $x$ . The  $m_x(H_{me})$  values have been deduced from Eq. (1). The solid lines are calculated using Eq. (2) with the following parameters:  $M_{eff} = 720 \text{ emu cm}^{-3}$ ,  $\gamma = 1.835 \times 10^7 \text{ s}^{-1}$ ,  $H_u = 30$  Oe, and  $H_b = 40$  Oe. Note that  $H_{me}$  is deduced from Figure 2. The sketches show how the magnetization direction rotates as function of the applied voltage.

$H_{me}(V)$  dependence previously determined (see Figure 2). This dependence highlights the well-known softening of the frequency when the magnetization rotates from a hard axis to an easy one;<sup>26</sup> the frequency minimum directly gives the voltage at which the system is in-plane isotropic (i.e., where  $H_{me}$  compensates the initial anisotropy field and the bias field). Both the experimental frequency and the amplitude dependencies are well fitted by the solid lines and they clearly show a  $90^\circ$  rotation of the magnetization direction. The theoretical values have been calculated by using a magnetic energy density of the film, where the indirect magnetoelectric field is modeled by a voltage dependent uniaxial anisotropy field. In these conditions, the following analytical expression of the frequency can be derived from the Smit-Beljers equation:<sup>15</sup>

$$\frac{2\pi f}{\gamma} = \sqrt{(H_{me}(V) - H_u)\cos 2\varphi + H_b \sin \varphi} \times \sqrt{4\pi M_s + H_b \sin \varphi + H_u \sin^2 \varphi + H_{me}(V) \cos^2 \varphi}, \quad (2)$$

where  $\varphi$  is evaluated at each increment of the applied voltage. Finally, it should be noted that the spectra profiles were not always close to a Lorentzian one, especially at high applied voltages, which make this modeling really robust.<sup>24,25</sup>

In summary, the indirect magnetoelectric coupling in artificial heterostructure was used to rotate the magnetization direction. MS-FMR was used in two different modes to: (i) quantitatively measure the voltage-dependence of the indirect magnetoelectric field (which is strain-induced by the piezoelectric actuator) and to (ii) observe the rotation of the magnetization. The voltage dependence of the  $H_{me}$  was found to be almost linear (in the range 0 V–200 V) and was

used during the frequency and amplitude variations of the sweep-frequency spectra modeling.

M.S.G. and C.T acknowledge Exploratory Research Project SPINTAIL PN-II-ID-PCE-2012-4-0315 and TUCN-MADSPIN Research Project for financial support.

- <sup>1</sup>N. A. Spaldin and M. Fiebig, *Science* **309**, 391 (2005).
- <sup>2</sup>S.-W. Cheong and M. Mostovoy, *Nat. Mater.* **6**, 13 (2007).
- <sup>3</sup>R. Ramesh and N. A. Spaldin, *Nat. Mater.* **6**, 21 (2007).
- <sup>4</sup>M. Bibes and A. Barthélémy, *Nat. Mater.* **7**, 425 (2008).
- <sup>5</sup>W. Eerenstein, N. Mathur, and J. Scott, *Nature* **442**, 759 (2006).
- <sup>6</sup>C.-W. Nan, M. I. Bichurin, S. Dong, D. Viehland, and G. Srinivasan, *J. Appl. Phys.* **103**, 031101 (2008).
- <sup>7</sup>N. X. Sun and G. Srinivasan, *Spin* **2**, 1240004 (2012).
- <sup>8</sup>J. Ma, J. Hu, Z. Li, and C.-W. Nan, *Adv. Mater.* **23**, 1062 (2011).
- <sup>9</sup>M. Gueye, F. Zighem, D. Faurie, M. Belmeguenai, and S. Mercone, *Appl. Phys. Lett.* **105**, 052411 (2014).
- <sup>10</sup>M. Weiler, A. Brandlmaier, S. Geprägs, M. Althammer, M. Opel, C. Bihler, H. Huebl, M. Brandt, R. Gross, and S. Goennenwein, *New J. Phys.* **11**, 013021 (2009).
- <sup>11</sup>F. Zighem, D. Faurie, S. Mercone, M. Belmeguenai, and H. Haddadi, *J. Appl. Phys.* **114**, 073902 (2013).
- <sup>12</sup>J. H. Park, J.-H. Lee, M. G. Kim, Y. K. Jeong, M.-A. Oak, H. M. Jang, H. J. Choi, and J. F. Scott, *Phys. Rev. B* **81**, 134401 (2010).
- <sup>13</sup>C. Thiele, K. Dörr, O. Bilani, J. Rödel, and L. Schultz, *Phys. Rev. B* **75**, 054408 (2007).
- <sup>14</sup>C. Bihler, M. Althammer, A. Brandlmaier, S. Geprägs, M. Weiler, M. Opel, W. Schoch, W. Limmer, R. Gross, M. S. Brandt, and S. T. B. Goennenwein, *Phys. Rev. B* **78**, 045203 (2008).
- <sup>15</sup>F. Zighem, A. El Bahoui, J. Moulin, D. Faurie, M. Belmeguenai, S. Mercone, and H. Haddadi, *J. Appl. Phys.* **116**, 123903 (2014).
- <sup>16</sup>M. Gueye, B. M. Wague, F. Zighem, M. Belmeguenai, M. S. Gabor, T. Petrisor, C. Tiusan, S. Mercone, and D. Faurie, *Appl. Phys. Lett.* **105**, 062409 (2014).
- <sup>17</sup>S. Li, J. Xu, Q. Xue, H. Du, Q. Li, C. Chen, R. Yang, S. Xie, M. Liu, T. Nan, N. X. Sun, and W. Shao, *J. Appl. Phys.* **117**, 17B722 (2015).
- <sup>18</sup>M. Belmeguenai, H. Tuzcuoglu, M. Gabor, T. Petrisor, Jr., C. Tiusan, D. Berling, F. Zighem, T. Chauveau, S. Chérif, and P. Moch, *Phys. Rev. B* **87**, 184431 (2013).
- <sup>19</sup>W. Wang, H. Sukegawa, R. Shan, S. Mitani, and K. Inomata, *Appl. Phys. Lett.* **95**, 182502 (2009).
- <sup>20</sup>M. S. Gabor, M. Belmeguenai, F. Zighem, S. M. Chérif, T. Petrisor, Jr., T. Petrisor, C. Tiusan, and M. Hehn, *Spin* **4**, 1440022 (2014).
- <sup>21</sup>F. Zighem, Y. Roussigné, S. M. Chérif, and P. Moch, *J. Phys.: Condens. Matter* **20**, 125201 (2008).
- <sup>22</sup>J. Ben Youssef, N. Vukadinovic, D. Billet, and M. Labrune, *Phys. Rev. B* **69**, 174402 (2004).
- <sup>23</sup>F. Zighem, M. Belmeguenai, D. Faurie, H. Haddadi, and J. Moulin, *Rev. Sci. Instrum.* **85**, 103905 (2014).
- <sup>24</sup>G. Counil, J.-V. Kim, T. Devolder, C. Chappert, K. Shigeto, and Y. Otani, *J. Appl. Phys.* **95**, 5646 (2004).
- <sup>25</sup>G. Counil, J.-V. Kim, T. Devolder, P. Crozat, C. Chappert, and A. Cebollada, *J. Appl. Phys.* **98**, 023901 (2005).
- <sup>26</sup>F. Zighem, Y. Roussigné, S. M. Chérif, and P. Moch, *J. Phys.: Condens. Matter* **19**, 176220 (2007).